Pergamon

Acta mater. 49 (2001) 3621–3634

Acta MATERIALIA

www.elsevier.com/locate/actamat

STRAIN–TEMPERATURE BEHAVIOR OF NiTiCu SHAPE MEMORY SINGLE CRYSTALS

H. SEHITOGLU[1]†, I. KARAMAN[1], X. ZHANG[1], A. VISWANATH[1], Y. CHUMLYAKOV[2] and H. J. MAIER[3]

[1]University of Illinois, Department of Mechanical and Industrial Engineering, 1206 West Green Street, Urbana, IL 61801, USA, [2]Siberian Physical-Technical Institute, Revolution Square 1, 634050, Tomsk, Russia and [3]University of Paderborn, Lehrstuhl f. Werkstoffkunde, D-33095 Paderborn, Germany

(Received 26 December 2000; accepted 8 May 2001)

Abstract—Single crystal specimens of NiTi10Cu alloys were subjected to temperature cycling conditions under constant tensile and compressive stresses and the transformation strains were monitored. The [111] orientation exhibited the highest experimental transformation strains (6.64%) in tension while the [001] provides the highest transformation strains in compression (5.34%). These transformation strain levels are significantly higher than previously reported values on NiTiCu alloys. The theoretical treatment includes both the calculation of the CVP (correspondent variant pair) formation strain incorporating the growth of monoclinic phase from the most favorably oriented orthorhombic variant, and the concomitant detwinning of the monoclinic martensite. The experimental transformation strain values are consistently below the theoretical levels due to two main reasons: the slip deformation in the austenite domains as confirmed with TEM studies, and the incomplete transformation resulting in a mixture of orthorhombic and monoclinic phases as determined from diffraction patterns. The experimental transformation strains are higher in tension compared to compression for most single crystal orientations due to two factors: the additional strain associated with the detwinning of the B19′phase in the final microstructure (such as in [111] case), and the partial completion of the second step of the transformation limiting the compression strains. *© 2001 Acta Materialia Inc. Published by Elsevier Science Ltd. All rights reserved.*

Keywords: Shape memory; Martensite; Single crystal; Transmission electron microscopy (TEM); Phase transformations

1. INTRODUCTION

Previous work by the author and his colleagues focussed on compression deformation behavior of NiTiCu alloys [1]. In these early experiments the temperature was maintained at room temperature and the strain was progressively increased to as much as 8%. Transformation strains (pseudoelastic and shape memory) were determined as a function of crystal orientation. The results showed that the experimental transformation strains in compression were confined to 4% in most single crystal orientations. This value is significantly lower than the theoretically possible values of transformation strain. The NiTi10Cu alloys undergo a two step transformation strain compared to the NiTi alloys. The lower values of transformation strain were attributed to incomplete transformation resulting in a mixture of B19 (orthorhombic martensite) and B19′ (monoclinic martensite) phases in the final microstructure, and the inelastic deformation in austenite domains limiting the recoverability [1]. To interrogate the upper limit in transformation strains, a new type of experiment, involving thermal cycling under stress holds, has been undertaken in the present study. This type of experiment allows the study of transformation strains as high as 6.64% in this study. Also, in the uniaxial straining cases the two steps of the transformation were not apparent, while in the present study it can be viewed more clearly through the changes in the slope of the strain–temperature curves.

In previously published results in the literature on NiTi10Cu polycrystals [2–4], the thermal cycling experiments have been conducted under tension loading conditions only. In the current work, by studying the deformation under both the tensile and compressive stress holds, it was possible to obtain definitively the transformation strains under both conditions. Larger transformation strains (6.64%) were realized upon the use of single crystals in the present study

† To whom all correspondence should be addressed. Tel.: +1-217-333-1176; fax: +1-217-244-6534

E-mail address: huseyin@uiuc.edu (H. Sehitoglu)

1359-6454/01/$20.00 © 2001 Acta Materialia Inc. Published by Elsevier Science Ltd. All rights reserved.
PII: S1359-6454(01)00192-6

compared to the 3.5% strain reported on polycrystals [2–4] by other researchers. The magnitude of the transformation strains measured under constant stress conditions are near the theoretical values in some of the orientations (such as [111] and [001]) and stress directions but lower than the theoretical values in others due to slip deformation. Theoretical transformation strain calculations for both stages of the transformation and the detwinning strain for the B19′ structure are included for comparison and interpretation of experimental results. The theoretical transformation strain corresponds to the formation of a CVP (correspondent variant pair) which is an ensemble of two twin related martensite variants. The detwinning refers to the growth of one of the variants within a CVP with respect to the other. Upon complete detwinning, a single crystal of martensite is created.

Despite the potential interest in the NiTi10Cu alloys, there has been significantly less work reported compared to the extensive literature on binary NiTi alloys. These alloys undergo a single transformation step (cubic to monoclinic) for Cu contents less than 8%. For Cu contents near 10% the two stage transformation has been observed [3, 4]. For Cu contents exceeding 10% a single step transformation (cubic to orthorhombic) prevails. Some of the advantages of these alloys include a nearly constant M_s temperature with slight compositional changes, and pseudoelastic response at room temperature without the need for the aging treatment. It is believed that the Cu in solid solution in the form of clusters raise M_s temperature to levels near −30°C. Saburi and colleagues [2] have conducted temperature cycling experiments on NiTiCu under constant tensile stress and established the transformation strain and the habit plane direction. Because the transformation direction unit vector was unknown it was not possible to establish RSSF (resolved shear stress factors) and the corresponding transformation strains. Moberly [4] also subjected NiTi10Cu wires to thermal cycling under constant tensile stress in the range 50 to 100 MPa and noted the two-stage transformation behavior characteristic of this system. Moberly [4] observed that the first transformation associated with cubic to orthorhombic phase steers the second step of the transformation. This is different than the case of a single step cubic to monoclinic martensite formation typical of binary NiTi alloys. As mentioned earlier, the transformation strain obtained by these two groups of researchers has been limited to 3.5%.

Chumlyakov and colleagues [5] were the first to explore the behavior of single crystals of NiTi10Cu in [001], [011] and [111] orientations. By examining the stress–strain behavior, they reported strong orientation dependent behavior in these alloys as well as asymmetry between tension and compression. They found smaller transformation strain in compression compared to tension. They attempted to determine the transformation temperatures associated with each phase of the transformation based on resistivity measurements but were unable to resolve precisely all the transformation temperatures.

In summary, the present study has been designed to reveal the transformation strains in selected single crystal orientations of NiTi10Cu. Two orientations chosen, [122] and [012], represent the highest transformation strain theoretically possible in tension and compression respectively. As shown later, these orientations may not attain the maximum transformation strain due to supression of transformation via dislocation generation. The other three orientations studied, [001], [011] and [111], were selected to compare experiment with theory and to impart higher slip resistances compared with the [122] and [012] cases. To shed further light into the results, incremental straining experiments in tension are reported for the [122] and [111] directions to understand the role of slip and fracture processes, respectively.

The current study also presents a complete theoretical solution of the two step (cubic to orthorhombic to monoclinic) transformation for both tension and compression cases. The growth of monoclinic martensite from the most favorably oriented orthorhombic variant was calculated. The role of detwinning on the transformation strains are also identified for both the single step and the two step transformation. The reason for higher transformation strains in tension compared to compression is partially attributed to the detwinning effect. When the detwinning is included the theoretical transformation strain levels attain values as high as 9.39% (in [122] case). This information has not been presented in previous studies and points out the potential of NiTiCu alloys for high transformation strain applications.

2. MATERIAL, EXPERIMENTAL RESULTS AND MICROSTRUCTURE

The material has been obtained from Specialty Metals, New Hartford, NY. It was cast to a specific chemical composition with atomic percentages as 49.5Ti, 9.1Cu and 41.4Ni. The material was then grown into single crystals in an inert environment using a Bridgman furnace. It was solutionized at 920°C for 24 hours in a vacuum furnace and then furnace cooled. In early work [1], with close examination of the TEM results, we noted the presence of Cu clusters in solution.

The specimens were tested under thermal cycling using dog bone specimens. The experiments were conducted under stress control and a miniature extensometer was used to measure the axial deformation during the experiments. In all the experiments the temperature was cycled between −120°C and 120°C. The duration of heating and cooling was approximately 60 minutes per cycle to minimize transient effects and thermal gradients. Five crystallographic orientations were examined: [001], [011], [111], [012] and [122]. A DSC (Differential Scanning

Calorimetry) analysis provided $A_f = 31°C$ and $M_f = -20°C$. These values are in qualitative agreement with the temperature cycling results reported hereupon accounting for the role of stress on the transformation temperatures.

TEM investigations expedite the understanding of the microstructure and the mechanisms that lead the experimental observations explained above. Since the favorable slip system in binary NiTi alloys is found to be <011>{100} or <001>{100} [8], the dislocation generation is harder to activate than the activation of martensitic transformation in the [001] orientation. Figure 1 indicates a dislocation free matrix after thermal cycling under compression with a monoclinic martensite variant supporting this conclusion. The figure clarifies why the [001] orientation does not experience significant ratcheting, and demonstrates near theoretical recoverable strain (5.4%), for instance, under 100 MPa compressive stress.

The two stages of deformation in the [111] orientation under tensile loads is attributed to the separable B2→B19 and B19→B19′ transformations. TEM observations support this conclusion as demonstrated in Fig. 2(a) from the [111] sample thermally cycled under 100 MPa tensile load. The figure shows a lamellar structure of the transformation products and the B2 matrix. Based on the diffraction pattern evaluation, it has been concluded that the lamellar features in this figure are monoclinic martensite variants. In the corresponding diffraction pattern, Fig. 2(b), reflections from the orthorhombic B19 martensite and one monoclinic B19′ martensite variant have been indexed, and marked "o" and "m", respectively. For the sake of clarity, the indices of the second monoclinic variant have been omitted. This variant is seen

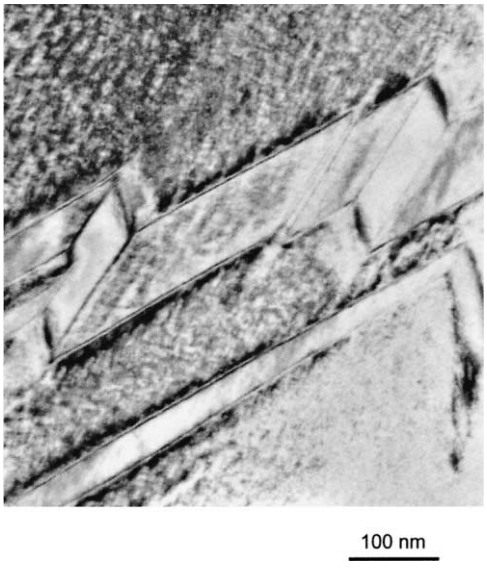

Fig. 1. A representative bright field image of the [001] orientation under 100 MPa compressive load, thermally cycled between −100°C and 100°C exhibiting a dislocation free matrix with a monoclinic martensite variant.

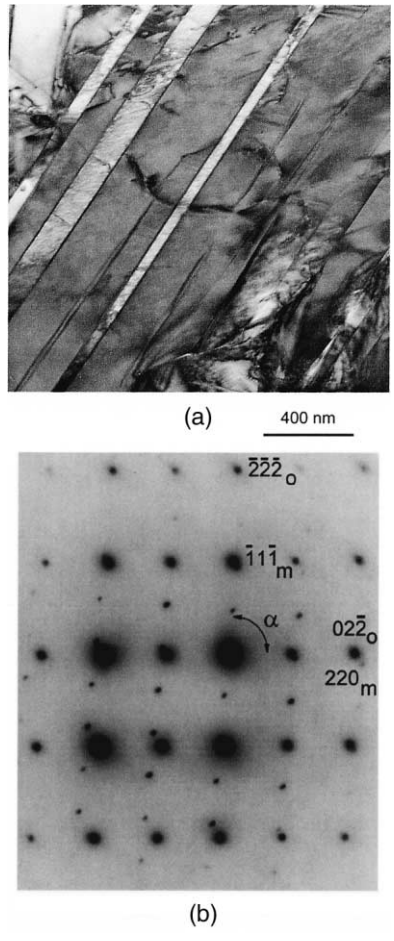

Fig. 2. (a) Bright field image of the [111] orientation thermally cycled in between −100°C and 100°C under 100 MPa tensile load. (b) Corresponding selected area diffraction pattern indicating the presence of orthorhombic B19 martensite and two variants of monoclinic B19′ martensite. See main text for details.

along the [010] zone axis and gives rise for many of the weaker reflections. The different types of martensite are best distinguished if the sample is tilted such that diffraction patterns from the <001> zone axis are obtained [4]. Given the limited tilt angle available in the TEM, this was not possible for the [111] oriented sample. For foil orientations different than <001> the diffraction patterns are rather similar. Note that the angle, α, in Fig. 2(b) is 87° and 89° for the orthorhombic and the monoclinic martensite, respectively. Thus, diffraction patterns were evaluated in the present study based on the computer simulations that employed angles, distances and relative intensities of the reflections.

The small ratcheting between cycles in the [111] orientation is a result of small dislocation activity in the B2 phase. However, the slip activity is so small that this does not have a significant effect on the recoverable strain (to be discussed later under Fig. 8), and also the detwinning contributes to the overall transformation strain in this case. On the other hand,

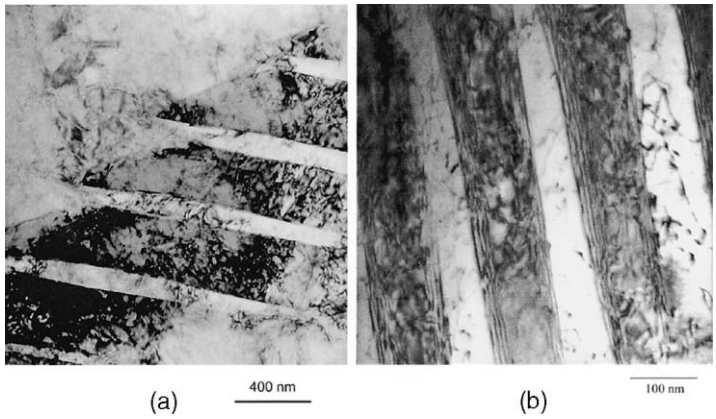

Fig. 3. (a) A TEM image of the [122] orientation thermally cycled between −100°C and 100°C under 90 MPa tensile load. The martensite variant lies diagonally in this photograph with internal twinning. (b) Another monoclinic martensite lamellae from a different region with a significant dislocation density. The martensite and austenite regions are dark and light regions, respectively. The dislocation activity in both (a) and (b) is the foremost reason for the ratcheting and notable irrecoverability in this orientation.

the [122] orientation under tensile load holds demonstrate significant irrecoverable strains and ratcheting during thermal cycling between −100°C and 100°C (Fig. 9). A typical microstructure of the [122] case is shown in Fig. 3(a). The high dislocation activity in the lamellae as shown in Figs 3(a) and (b) (from another area with higher magnification and different diffraction conditions) is thought to be the origin of the ratcheting and the irrecoverability as the interaction between dislocations and the martensite hinders the back transformation of the product phase.

3. CALCULATION OF THEORETICAL TRANSFORMATION STRAINS

To understand the theoretical results, it is informative to study the schematic shown in Fig. 4. The austenitic (parent) phase is cubic and is denoted as B2 and the monoclinic martensite is denoted as B19′. The intermediate phase, B19, is orthorhombic martensite. The growth of B19′ from the orthorhombic B19 phase is illustrated in this figure. The habit plane between the B2 and B19 phases is denoted as **m** and the transformation direction is denoted as **b**. Note that **b** is not a unit vector and includes the transformation magnitude. The B19 martensite is essentially twinless. The B19′ has an internally twinned structure, called the correspondent variant pair (CVP), with the volume fraction of twins denoted as f and $1-f$ respectively. The correspondent variant pair (CVP) refers to the ensemble of two twin related martensite variants. The twin plane within the B19′ is denoted as **n** and the twinning shear direction is given as **a**. The habit plane and the transformation direction for the B19′ are denoted as **m** and **b**, respectively. As the transformation proceeds, both the B19 and B19′

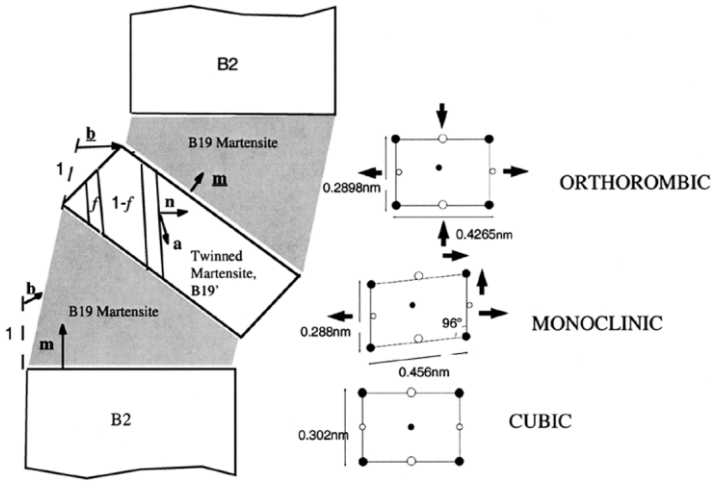

Fig. 4. A schematic showing the transformation planes and directions associated with successive step transformation in NiTi10Cu alloys under tensile loadings. The lattice constants for the three crystal structures are included.

domains grow in expense of the parent phase B2. At the conclusion of the transformation B19′ prevails over the microstructure but residual B19 phase has also been observed. The detwinning of the B19′ occurs with further cooling (or under stress) where the smaller twin volume fraction is absorbed by the major twin volume fraction within the CVP. As a result the B19′ phase becomes a single crystal. In order to determine the transformation strains associated with each step of the transformation all the transformation planes and directions need to be evaluated. Finally, to establish the detwinning strain one needs to know the twin volume fractions and the twin plane and direction.

We note in Fig. 4, in addition to the transformation parameters, the crystal structures and their lattice constants are also provided. The schematic of these crystal structures are viewed from the [001] cubic direction. During transformation from cubic to orthorhombic the lattice is compressed and extended in two respective directions, followed by shear and expansion during orthorhombic to monoclinic transition. The arrows attached to the drawings indicate the deformations associated with the transformations.

Initially, we study the first step of the transformation. The lattice correspondences for the transformation from cubic to orthorhombic are $[0\ 0\ 1]_c \leftrightarrow [1\ 0\ 0]_o$, $[1\ \bar{1}\ 0]_c \leftrightarrow [0\ 1\ 0]_o$, $[1\ 1\ 0]_c \leftrightarrow [0\ 0\ 1]_o$ [2]. There are six independent lattice correspondence variants for the B19 martensite. The lattice constants for the orthorhombic phase were obtained from Ref. 4. For the 10% Cu alloy, these parameters are [4]: $a = 0.2898$ nm, $b = 0.4265$ nm, $c = 0.4514$ nm. The cubic phase has the lattice constant $a_0 = 0.302$ nm. The habit plane normal and the transformation direction for the B2→B19 transformation are determined based on Energy Minimization Theory [6, 7]. The habit plane normal is $\mathbf{m} = \{0.6403,0.5423,0.5439\}$ and the transformation direction is $\mathbf{b} = <0.0648,0.0499,0.0500>$. The solutions for the twin volume fractions are $f = 0.9753$ and 0.0247 rendering the orthorhombic phase essentially twinless.

The corresponding transformation strain is given as

$$\boldsymbol{\epsilon} = \frac{1}{2}(\mathbf{F}_M^T \cdot \mathbf{F}_M - \boldsymbol{I}) = \frac{1}{2}[\mathbf{b}\otimes\mathbf{m} + \mathbf{m}\otimes\mathbf{b} + (\mathbf{b}\cdot\mathbf{b})\mathbf{m}\otimes\mathbf{m}] \tag{1}$$

where $\mathbf{F}_M$ is the deformation gradient matrix. In equation (1) the third term represents contribution from finite deformation effects. Given the strain tensor in equation (1), the elongation along a prescribed loading direction denoted by $\boldsymbol{e}$ can be determined as follows

$$E_1 = \boldsymbol{e} \cdot \boldsymbol{\epsilon} \cdot \boldsymbol{e} \tag{2}$$

The transformation strain contours corresponding to the cubic to orthorhombic transformation are included as the first column in Figs 5(a) and (b) for tension and compression respectively.

In the second step of the transformation, B19→B19′, the growth of the monoclinic martensite (B19′) within the orthorhombic martensite (*B*19) was analyzed. The lattice parameters of the B19′ martensite are obtained from Moberly *et al.* [4] ($a = 2.88$ Å, $b = 4.226$ Å, $c = 4.56$ Å and $\beta = 96.6°$) The twin plane is determined as $\mathbf{n} = \{0.7171,0,0.6970\}$ for Type II-1 twinning. Corresponding to these twinning planes, the twinning shear directions are calculated as $\mathbf{a} = <0.0089,0.2239,0.0083>$. The habit plane and the transformation direction for the second step of the transformation can not be classified into a single family. The resultant twin volume fractions, *f*, differ depending on the active orthorhombic variants producing different final monoclinic variants. For each possible solution of the twin volume fraction there is a corresponding habit plane normal and transformation vector. The transformation strain for this step is given similar to equation (1), but **b** and **m** are used which represent the deformation of the active orthorhombic martensite. We obtain

$$\begin{aligned}\boldsymbol{\epsilon} &= \frac{1}{2}[(\mathbf{F}\mathbf{F}_M{}^{-1})^T \cdot (\mathbf{F}\mathbf{F}_M{}^{-1}) - \mathbf{I}) \\ &= \frac{1}{2}[\mathbf{b}\otimes\mathbf{m} + \mathbf{m}\otimes\mathbf{b} + (\mathbf{b}\cdot\mathbf{b})\mathbf{m}\otimes\mathbf{m}]\end{aligned} \tag{3}$$

where **F** is the deformation gradient associated with the orthorhombic to monoclinic transformation. The results for the orthorhombic to monoclinic martensite in tension and compression are shown on the right hand side of Figs 5(a) and (b), respectively. It is noted that the magnitude and the orientation dependence of maximum transformation strain differ between the tension and compression cases. We note that in the case of tension Fig. 5(a) the first step of the transformation dominates. In the second step of the transformation for tension some of the orientations in the lower portion of the triangle exhibit negative values. This means that the second step of the transformation can not occur in these orientations and should be taken as zero. For the case of compression (Fig. 5(b)), the transformation strains are indicated with negative numbers. Contrary to the tension case, the transformation strains in compression are higher for the second step of the transformation.

Now, we consider the transformation from cubic to monoclinic in a single step. Using the same lattice parameters of cubic and monoclinic phases as above, we obtain the same twin plane and twin shear solutions for the single step transformation as the two step transformation. Contrary to the two step case, unique solutions for *f* are obtained. Corresponding to an *f* of 0.1315 for Type II-1 twins, we obtain $\mathbf{m} = \{0.9002,0.3404,0.2716\}$ and $\mathbf{b} = <0.0614,0.0838,0.1015>$. Corresponding to the solution of $f = 0.8685$ the theory yields

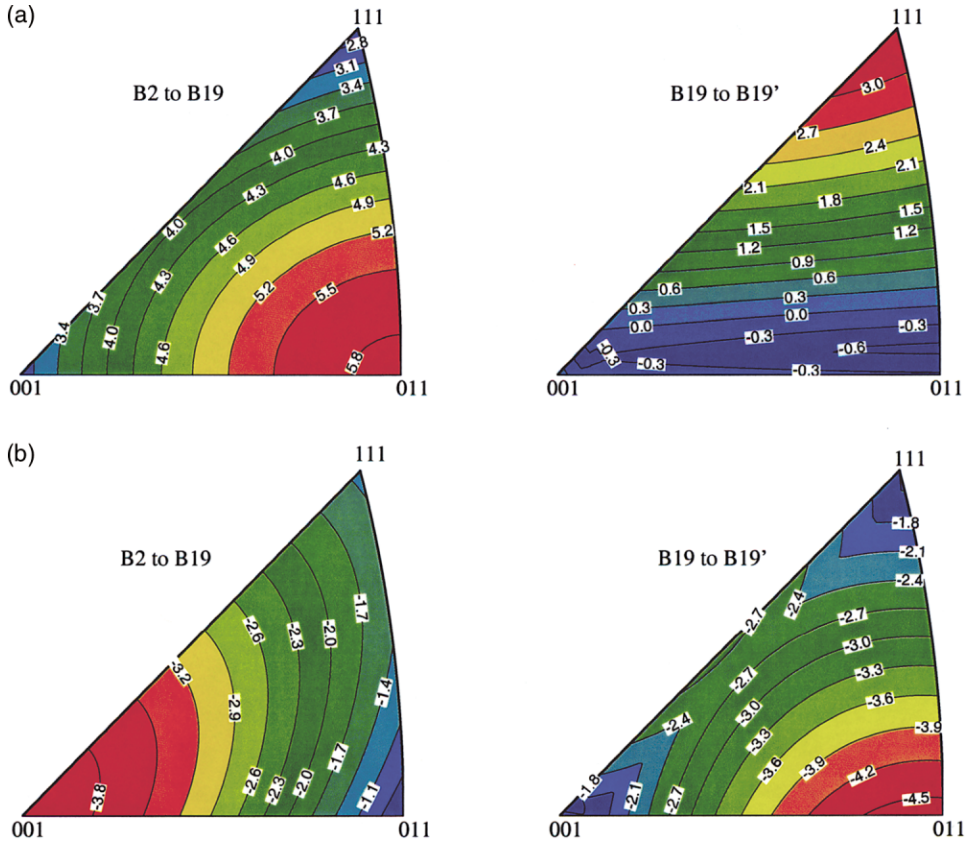

Fig. 5. (a) Strains associated with B2→B19 and B19→B19′ transformation (tension). (b) Strains associated with the two step (B2→B19 and B19→B19′) transformation (compression).

m = {0.3564,0.5997,0.7165} and **b** = <0.1350,0.0433,0.0320>. The magnitude of shear |**b**| in both cases is 0.1451. The results for the transformation strains (CVP formation) for the single step transformation are given in Fig. 6. Both tension and compression results are included in Fig. 6. The results for the tension case show maximum transformation strains of 7.83% near [122], while in compression, the maximum transformation strains (6.37%) are near the [012].

In Figs 5 and 6 the transformation strains shown are for the formation of correspondent variant pairs (CVPs for Type II-1 twins). It is possible to determine the detwinning contribution to the transformation strain. The detwinning strain (conversion of the small volume fraction variant to the large one within the

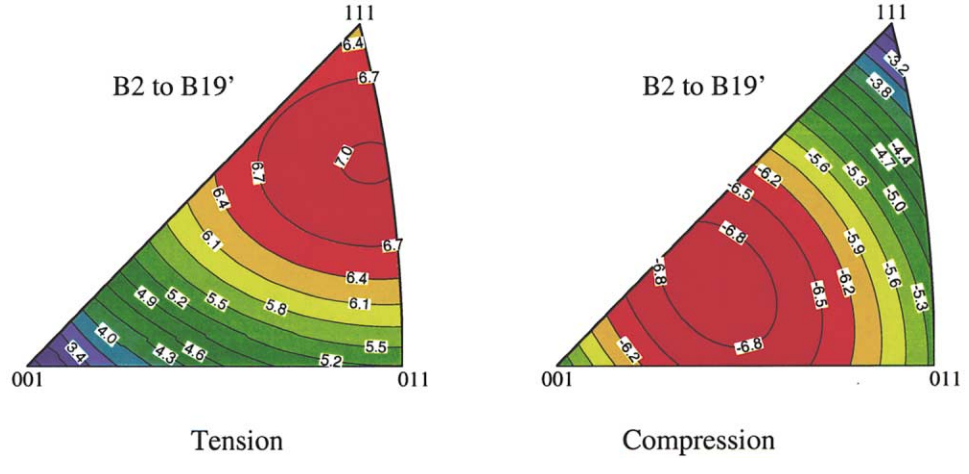

Fig. 6. Strains associated with B2→B19′ transformation (single step transformation).

Table 1. Transformation strains under tension (in percent)

	Two step transformation		Single step transformation	B19′ detwinning	
	B2→B19 cubic→orthorhombic	B19→B19′ orthorhombic→monoclinic	B2→B19′ cubic→ monoclinic	Single step	Two steps
[111]	2.55	3.49	7.05	8.67	8.33
[001]	2.78	0.70	2.98	2.98	3.49
[122]	4.64	2.60	7.83	9.39	8.71
[012]	5.01	0.41	5.32	6.19	6.32
[011]	5.57	0.44	5.87	7.00	7.14

CVP) can be determined as follows. The average deformation gradient matrix of a twinned martensite is written as,

$$\mathbf{F}_M = \mathbf{R}_h[f\mathbf{R}_{ij}\mathbf{U}_j + (1-f)\mathbf{U}_i)] \tag{4}$$

where $\mathbf{U}_i$ and $\mathbf{U}_j$ are the symmetric part of the deformation gradient matrices of the two variants in the twin, and $\mathbf{R}_h$ is the relative rotation between the twinned martensite and the parent phase.

The variant and $\mathbf{U}_j$ is converted to $\mathbf{U}_i$ if the volume fraction $f<0.5$. The deformation after detwinning is (by setting $f = 0$) obtained as

$$\mathbf{F}_M^{dt} = \mathbf{R}_h\mathbf{U}_i \tag{5}$$

If the volume fraction f is greater than 0.5, variant $\mathbf{U}_i$ converts to $\mathbf{U}_j$ and the transformation including detwinning is given by setting $f = 1$ as,

$$\mathbf{F}_M^{dt} = \mathbf{R}_h\mathbf{R}_{ij}\mathbf{U}_j = \mathbf{R}_h\cdot(\mathbf{U}_i + \mathbf{a}\otimes\mathbf{n}). \tag{6}$$

Once $\mathbf{F}_M^{dt}$ is known, the transformation strain (including CVP formation and detwinning) can be determined similar to equation (2) with $\mathbf{F}_M$ replaced by $\mathbf{F}_M^{dt}$.

The transformation strains in tension and compression for the five orientations studied in this work are summarized in Tables 1 and 2, respectively. In addition to the strains associated with the correspondent variant pair (CVP) formation, the strain associated with detwinning of the monocline martensite obtained via single step and via two steps are included in Tables 1 and 2. We note that the detwinning strains in tension exceed 2%in the [111] and [122] orientations for the two step case while they are nearly zero in compression cases. We also note that in the case of two step transformations the transformation strains differ from the single step case. This difference exists both for CVP formation and for the accompanying detwinning strains. The difference in detwinning amounts between the single and the two step transformation is expected based on the transformation parameters of the resultant martensites and their respective twin volume fractions.

The slip system in the austenite (B2 phase) has been identified as {100}<001> and {100}<011> by Chumlyakov and colleagues [8] from burgers vector measurements. The Schmid factor contours associated with these systems are given in Fig. 7(a). These figures clearly identify the [001] direction as having a zero Schmid factor ruling out plastic deformation in this orientation. We note that the Schmid factors in other orientations permit different degrees of dislocation glide.

4. EXPERIMENTAL RESULTS—STRAIN–TEMPERATURE RESPONSES

To illustrate the experimental results under temperature cycling conditions, we consider the schematic shown in Fig. 7(b). In the case of a constant value of applied stress, the strains increase upon cooling and the first step of the transformation commences at a temperature designated as M_s^1. The superscripts 1 and 2 refer to Steps 1 and 2 respectively. Upon further cooling (and depending on the orientation and the stress level), a second stage of the transformation appears and this transformation pro-

Table 2. Transformation strains under compression (in percent)

	Two step transformation		Single step transformation	B19′ detwinning	
	B2→B19 cubic→orthorhombic	B19→B19′ orthorhombic→monoclinic	B2→B19′ cubic→ monoclinic	Single step	Two steps
[111]	−1.38	−1.18	−2.34	−2.36	−2.56
[011]	−4.15	−1.25	−4.68	−4.68	−5.4
[122]	−1.61	−2.60	−4.08	−4.09	−4.21
[012]	−2.89	−3.67	−6.37	−6.37	−6.56
[011]	−0.85	−4.33	−4.91	−4.91	−5.18

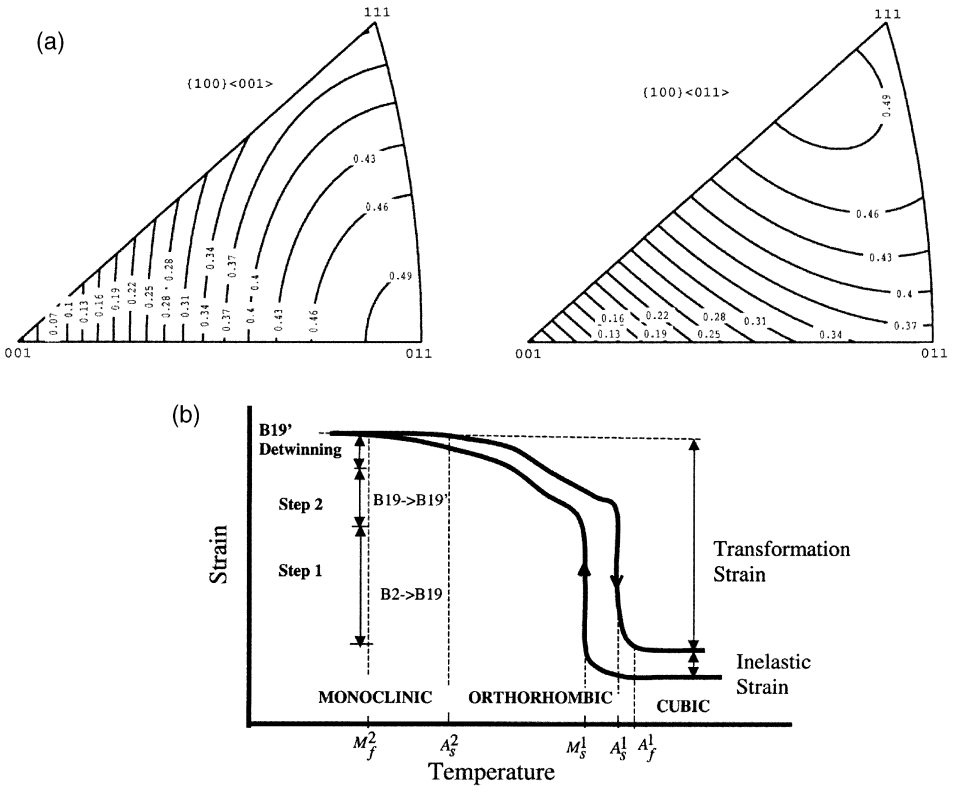

Fig. 7. (a) Schmid factors associated with {100}<001> and {100}<011> slip systems in NiTiCu alloys. (b) A schematic showing successive step transformation and detwinning in NiTi10Cu alloys under tensile loadings.

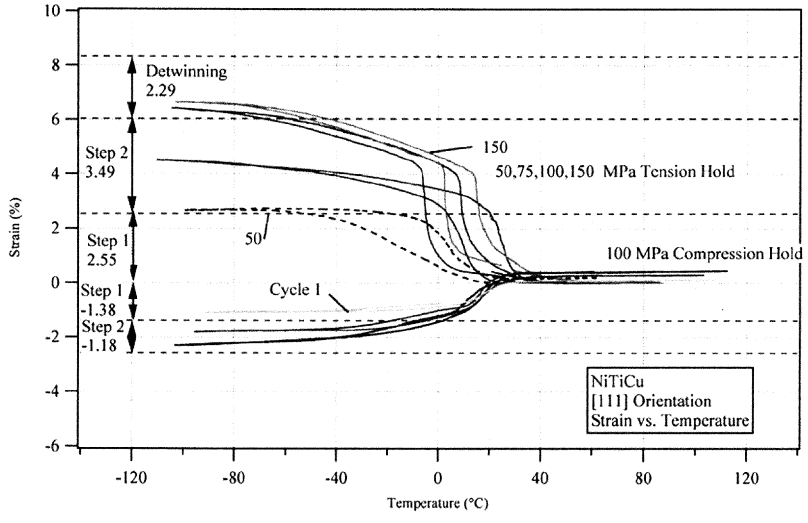

Fig. 8. Transformation strain–temperature variation under thermal cycling for the [111] tension case with stress levels in the range 50–150 MPa. Note that if the detwinning strain is included the theoretical transformation strains reach 8.33% in tension.

ceeds until the martensite finish temperature M_f^2 is reached. The detwinning of the monoclinic martensite contributes further to the transformation strains. Upon heating, the transformation occurs in the reverse order, starting at A_s^2, firstly as monoclinic to orthorhombic transformation followed by the orthorhombic to cubic transformation. The transformation to austenite is completed at A_f^1. The overall transformation strain is the sum of the transformation associated with both steps of the transformation and the detwinning strain. Depending on the applied stress level, slip deformation develops during temperature cycling producing inelastic (irrecoverable) strains. It is important to subtract this portion of the strain from the overall

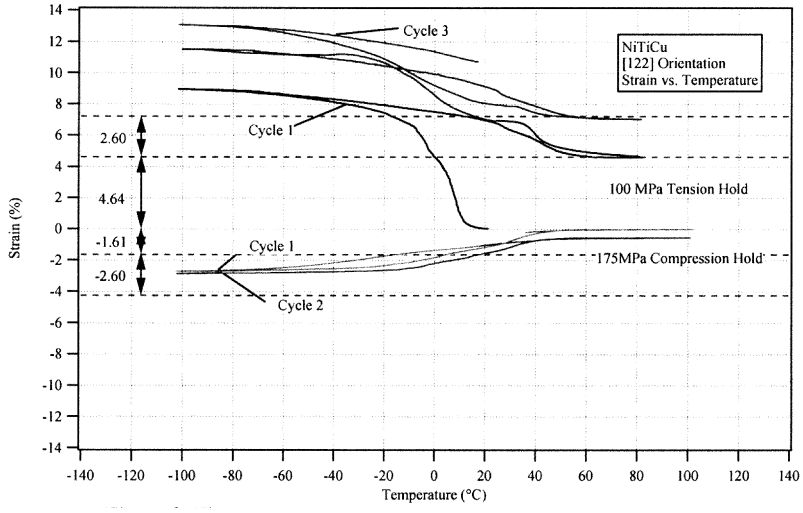

Fig. 9. The strain–temperature response for the [122] orientation.

measured strain to determine the transformation strain. The results for compression are similar to those shown in Fig. 7(b) but the strain scale is reversed, and the detwinning strain is negligible. The actual experimental results may not follow the strain–temperature path displayed in Fig. 7(b) because the two steps of the transformation and the detwinning can not be separated or in some cases the second step has not been observed all together.

We first consider the transformation strain variation with temperature cycling for the [111] case under tensile stress levels of 50, 75, 100 and 150 MPa. This is shown in the upper portion of Fig. 8. The results correspond to the saturated strain–temperature response obtained after two to three cycles. In the lower portion of Fig. 8, compressive stress results for 100 MPa are shown. The theoretical transformation strains associated with the first step (cubic to orthorhombic), the second step (orthorhombic to monoclinic) of the transformation and the detwinning of the monoclinic phase are indicated with dashed horizontal lines. These values are 2.55%, 3.49% and 2.29% for tension respectively. For the case of 150 MPa, the experimental transformation strain is as high as 6.64%. Since this value exceeds the transformation strain of 6.04% based on the CVP formation, it is apparent that partial detwinning of the martensite has occurred and the experimental results approach the theoretical limit of 8.33% (see Table 1). If the stress levels exceed 150 MPa the transformation strains do not increase further. In the 50 MPa case the two stages of transformation are not as noticeable and it appears that only the first stage of the transformation occurred. As the stress level is progressively increased the transformation strains reached upon cooling also increased. The 75 MPa and 100 MPa cases reside between the 50 MPa and 150 MPa extremes. We note that under compression (Fig. 8) the direction of the transformation is reversed and the transformation strains are much lower compared to tension. In compression, upon cooling the gage section of the specimen contracts and upon heating the transformation strains produce expansion. The two stage transformation is not visible in this case and the transformation strains are limited to 2.5%. The experimental transformation strains in compression observed in Fig. 8 are consistent with theoretical predictions shown in Table 2. We note that in addition to the transformation strains the presentation such as Fig. 8 provides a direct evidence on the role of stress on transformation temperatures.

Several experiments were conducted under thermal cycling with zero stress (not reported here). In these cases, the measured strains were less than 0.2%. Because of the self accomodating nature of the martensite variants, the measured strain of 0.2% reflects the small change in volume that occurs upon austenite to martensite transformation. Thermal cycling under stress allows the growth of selected variants in expense of others producing higher transformation strains.

The results of experiments on the [122] orientation are given in Figs 9 and 10. In the first set of experiments (Fig. 9) on the [122] orientation, the tensile stress level of 100 MPa produced considerable inelastic deformation. We note that the maximum strain in this case extends to levels in excess of 10% but the recoverable portion of the transformation strain is limited to 4.35%. This value is obtained upon subtracting the minimum strain reached in Cycle #1 (4.60%) from the maximum strain reached in the same cycle (8.95%). This is a lower recoverable transformation strain compared to the 6.5% established for the [111] case, and is lower than the theoretical values (7.83% for single step, and 7.24% for two step CVP formation strains) from Table 1. Also, the inelastic strain accumulates progressively with increasing number of cycles (Cycles 1 and 3 marked in Fig. 9). When inelastic deformation occurs during the thermal cycling it is difficult to partition the two

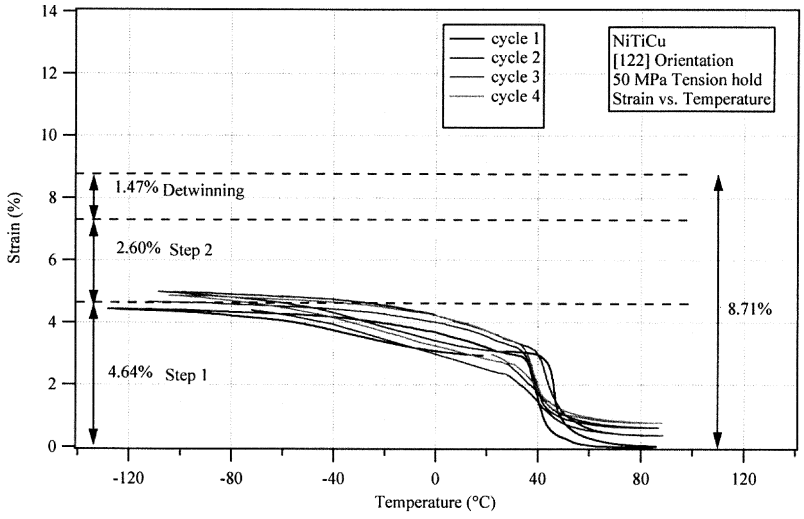

Fig. 10. Transformation strain–temperature variation under thermal cycling with a tensile hold of 50 MPa [122] case. The 1.47% increment corresponds to detwinning strain.

steps of the transformation. In the experiments, the stress level was progressively decreased from 100 MPa to 50 MPa to limit the inelastic strain. The strain–temperature variation under 50 MPa tension is shown in Fig. 10. The theoretical results are shown with first and second step of the transformation as well as the detwinning strain. The transformation strain levels in this case are 4.58%. The data from all four cycles is included to demonstrate the small amount of ratchetting that has occurred from Cycles #1 to #4. It is interesting to note that if the [111] and [122] results were compared solely based on the 50 MPa tension cases, the maximum transformation strain levels are higher in the [122] case compared to the [111] case, whereas the opposite is true for higher applied tensile stresses.

We now consider the [012] and [001] cases. The results for the [012] case are provided in Fig. 11. The experimental transformation strains in tension in this crystal orientation is 5.6%. This level is higher than the transformation strain for CVP formation but lower than the transformation strain of 6.3% including detwinning effects (Table 2). The results of experimental transformation strains (nearly 3.86%) in compression are also shown in Fig. 11 and this value falls short of the theoretical estimates near 6.5%. The strain–temperature response for the case of [00l] direction is given in Fig. 12. The case of [001] tension produces small transformation strains (1.32%), and in the case of [001] compression the experimental transformation strain is 5.34%. The transformation strains in compression are comparable to the theoretical predictions (5.4%). In both cases the strains do not exhibit a clear two stage transformation partially because the first step of the transformation dominates the transformation strain.

Finally, we consider the [011] case in Fig. 13. The [011] orientation tensile stress hold case provides

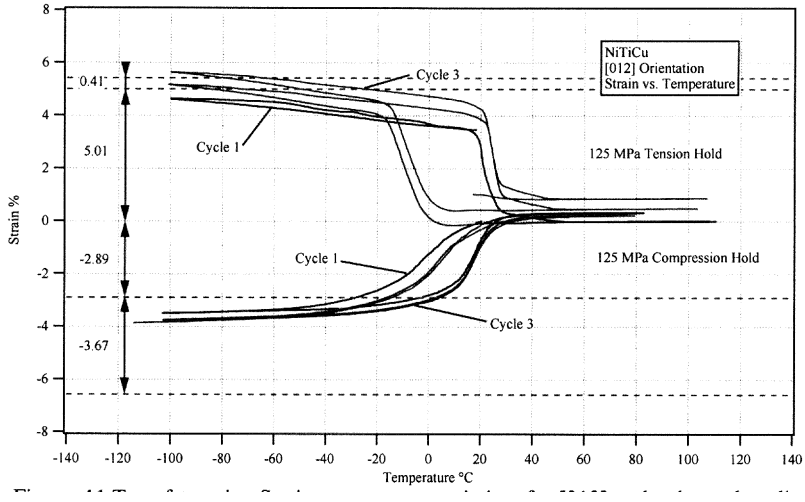

Fig. 11. Transformation strain–temperature variation for [012] under thermal cycling.

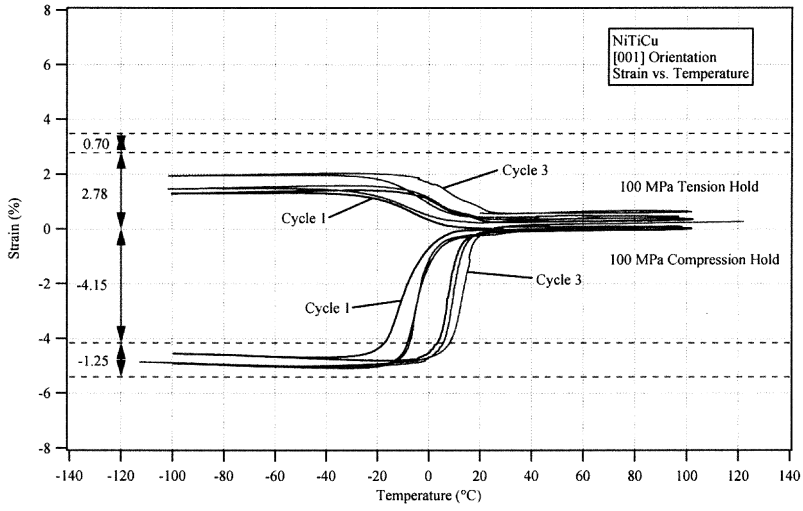

Fig. 12. Transformation strain–temperature variation for [001] under thermal cycling with a tensile hold of 100 MPa, and a compressive hold of −100 MPa.

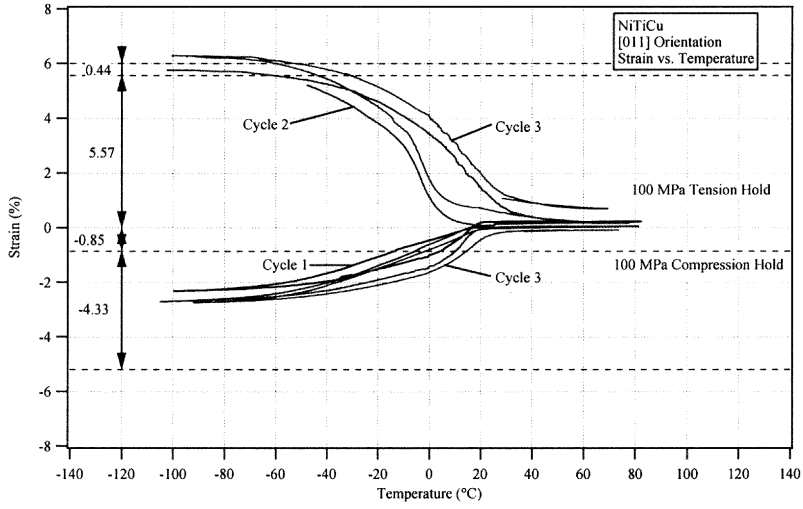

Fig. 13. Transformation strain–temperature variation for [011] under thermal cycling with a tensile hold of 100 MPa and a compressive hold of −100 MPa.

transformation strains at 5.76%. Small amount of ratchetting has occurred in tension and the experimental results are comparable to the theoretical calculations. The transformation strains in compression (2.7%) are significantly smaller than the theoretical values (5.18%).

To gain insight into the critical stress for transformation and the onset of slip deformation, the tensile stress–strain response of [122] and [111] crystals are shown in Figs 14 and 15. In these experiments, the applied strain is progressively increased, and after each cycle the specimen is heated to 100°C to recover the strain at zero stress. Both pseudoelastic strain and shape memory strain were measured and the transformation (recoverable) strain is the sum of these two strain components. The transformation strain is shown on the y-axis on the right hand side. They are 2.86% and 2.63% for [122] and [111] cases respectively. Two observations are noteworthy on Figs 14 and 15. The critical transformation stress for the [122] case is significantly lower than the [111] case. A lower transformation stress is a prerequisite for high transformation strains as long as slip deformation is curtailed. As noted in Figs 14 and 15, slip deformation occurs at much lower stress levels for the [122] orientation (second plateau) compared to the [111] case. The transformation strains in the [111] case have not reached their plateau level because fracture of the specimen occurred in the sixth cycle. We further note that the transformation strains in temperature cycling

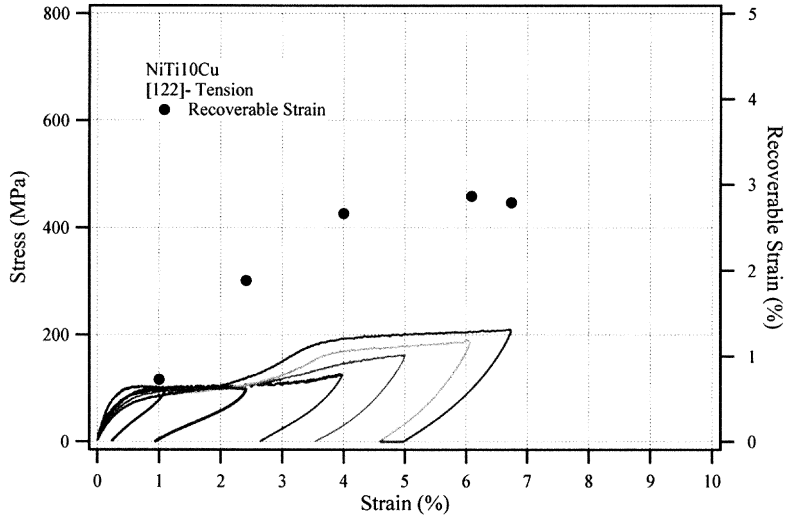

Fig. 14. Stress–strain response in tension under incremental straining for [122] orientation. The data points are the sum of shape memory strains obtained by heating the specimens to 100°C at zero stress and pseudoelastic strains.

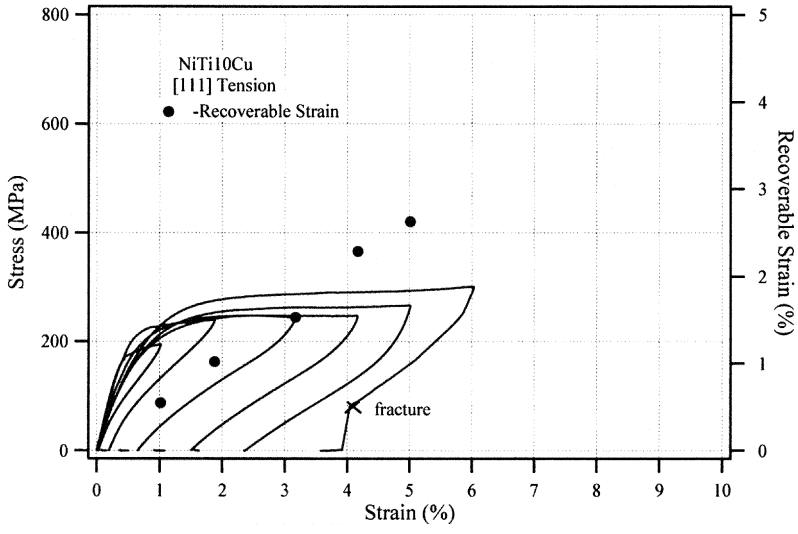

Fig. 15. Stress–strain response in tension under incremental straining for [111] orientation. The data points are the sum of shape memory strains obtained by heating the specimens to 100°C at zero stress and pseudoelastic strains.

experiments (Figs 8 and 9) far exceed those obtained under incremental straining experiments at constant temperature (Figs 14 and 15).

5. DISCUSSION OF RESULTS

The results provide significant evidence on the ability of the NiTiCu alloys to attain high transformation strains. Previous works [2–4] utilizing polycrystals have shown that the transformation strains are near 3.5%. In this study, much higher transformation strains (6.64%) were obtained which were comparable to those measured in the binary NiTi alloys [6]. We note that the polycrystalline forms of these alloys are highly textured with [111] texture and hence their behavior is similar to the [111] crystallographic direction. If the polycrystalline forms are textured with the preferred [001] orientation, these materials would be suited for applications involving primarily compression loadings. We further note that the results shed light into why the transformation strain in NiTiCu alloys are lower than aged NiTi alloys [6]. There are three main differences; the lattice constants are different resulting in a different transformation shear, the two stage transformation occurs in NiTi10Cu compared to single step transformation in NiTi, and the slip resistance of NiTi is higher because of the presence of impenetrable nickel rich precipitates

[6]. Potential heat treatments in NiTiCu could induce precipitates which could raise the slip resistance and increase the transformation strains.

The experimental transformation strain values in tension exceeded the levels in compression in most orientations. Two main reasons are forwarded to explain this difference. Firstly, based on theoretical calculations, the detwinning of the B19′ (monoclinic martensite) adds as much as 2.3% strain to the CVP formation strain under tensile loadings but has no effect in compression loadings. From Table 1, the detwinning strain is highest in the [111] direction. We note that the detwinning strain contribution in compression is nearly zero in the NiTiCu alloy studied (see Table 2). These results are markedly different than binary NiTi predictions [6] where detwinning strains in tension and compression are higher than the NiTiCu values. Secondly, the lower experimental strains in compression is attributed to incomplete transformation. The 'incomplete transformation' would affect the compression results more significantly than the tension case. This is because the major contribution towards the transformation strain in compression should occur during the second step. If this step is incomplete, the transformation strains are either confined to their first step values or lie between the first and the second step levels. The TEM observations (Fig. 2) confirm the existence of the two phase martensite lending credibility to the 'incomplete transformation hypothesis'.

The calculations for transformation strains are different than previous treatments in the following ways [6, 7]. The transformation strains are determined in a stepwise fashion where the orthorhombic phase influences the monoclinic phase formed at the conclusion of the transformation. The deformation gradient associated with the initial phase of the transformation enters the calculations as an initial strain in the matrix. For comparison purposes calculations are provided for single step transformation, two step transformation and the detwinning of the B19′ phase in both cases. A complete set of results are provided in Tables 1 and 2 that could be applied to alloys with Cu content less than 10% when a single step transformation was observed, and also to Cu contents exceeding 10% where only cubic to orthorhombic transformation has been shown to occur [5]. The theoretical results explain why the transformation strains for materials with high Cu contents decrease progressively when only cubic to orthorhombic transformation prevails.

We note that the inelastic flow during thermal cycling produces permanent deformation in the same direction as the applied stress. In other words, under tensile loadings the inelastic strain and the ratchetting strains are in the tensile directions, and the opposite is true for compression. To illustrate this behavior, we examined the strain temperature response of [122] orientation under a tensile stress of 100 MPa (Fig. 9). Upon heating from low temperatures to 100°C the material undergoes plastic flow and the resulting inelastic strain is tensile and exceeds 4%. When the cycling is continued the inelastic strain increment progressively accumulates. It is clear that the stress level needs to be reduced to limit inelastic flow in this orientation. Upon reducing the stress level to 50 MPa (Fig. 10), the ratchetting strain was reduced considerably. The slip deformation of the austenite phase occurs with the $\{100\}\langle 100\rangle$ and $\{100\}\langle 011\rangle$ dominant slip systems as established by Chumlyakov *et al.* [8]. Based on these slip systems the [001] orientation is least likely to undergo slip deformation. This opens the possibility of utilizing [001] texture to minimize ratchetting under cyclic loading. In fact, the highest transformation strains in compression were obtained in [001] orientation with 5.34% transformation strains.

It is worth comparing the current results with those reported previously on NiTiCu under compressive straining conditions by the authors [1]. In the previous study, the transformation strains in the compression case were limited to 4.1% in the [001] direction. The 4.1% transformation strain was the highest among all possible orientations in the previous work. In this work transformation strains in compression stress holds were 5.34%. We note that the use of thermal cycling experiments permits higher transformation strains to be measured compared to straining in tension. Tensile straining conditions produce stresses exceeding the constant stress levels utilized in this study and hence fracture of the samples could occur before higher strains are reached. To illustrate this point, we included the incremental straining in tension in the [111] direction (Fig. 15) where the strain in each cycle is progressively increased. But when the stress levels exceeded 250 MPa at strains near 6%, fracture followed and the transformation strain was limited to 2.63%.

6. CONCLUSIONS

1. The experimental transformation strains are higher in tension compared to compression for most single crystal orientations. The higher values of transformation strain in tension were attributed to two factors: the additional strain associated with detwinning of the B19′ phase in the final microstructure (such as in [111] case), and the larger transformation strain in the first step of the transformation in tension. The partial completion of the second step of the transformation limits the compression transformation strains to lower levels.
2. The transformation strain in NiTiCu alloys is limited by the activation of slip. The lack of precipitates lowers the slip resistance compared to aged NiTi alloys. Consequently, the formation of inelastic strain during thermal cycling bounds the transformation strain. The inelastic strain occurs when

the applied stress exceeds the critical transformation stress. Further heat treatments are expected to increase the flow resistance of austenite domains and allow the experimental transformation strains to approach the theoretical values.

3. The data obtained on the [111] tension and [001] compression cases opens the possibility to design materials with outstanding transformation strain capabilities. The lack of slip propensity in these orientations was confirmed with TEM studies, and the experimental transformation strains in both cases (6.64% and 5.34%, respectively) approached the theoretical values of 8.33% and 5.4%, respectively.

Acknowledgements—The research is supported by a grant from the Department of Energy, Basic Energy Sciences Division, Germantown, Maryland, DOE DEFG02-93ER14393 and the National Science Foundation contract CMS 99-00090, Mechanics and Materials Program, Arlington, Virginia. Professor Chumlyakov received support from the Russian Fund for Basic Researches, Grants No. 02-95-00350 and 03-99-32579. The facilities at Microanalysis of Materials, Materials Research Laboratory were used. This laboratory is funded by DOE-DMS grant DEFG02-96ER45439.

REFERENCES

1. Sehitoglu, H., Karaman, I., Kim, H., Zhang, X., Maier, H. J., Chumlyakov, Y. and Kireeva, I., *Metall. Mater. Trans. A*, 2001, **32A**, 477.
2. Nam, T. H., Saburi, T. and Shimizu, K., *Mater. Trans. JIM*, 1990, **31**(11), 959.
3. Moberly, W. J. and Melton, K. N., in *Engineering Aspects of Shape Memory Alloys*, ed. W. Duerig. Butterworth-Heinemann, 1990, p. 46.
4. Moberly, W. J., Duerig, T. W., Proft, J. L. and Sinclair, R., in *MRS Symp.*. 1992, p. 246.
5. Chumlyakov, Y., Kireeva, I. V., Zuev, Y. L. and Lyisyuk, A. G., *MRS Proc.*, 1997, **459**, 401.
6. Sehitoglu, H., Karaman, I., Anderson, R., Zhang, X., Gall, K., Maier, H. J. and Chumlyakov, Y., *Acta Materialia*, 2000, **48**(13), 331.
7. Ball, J. M. and James, R. D., *Arch. Rat. Mech. Anal.*, 1987, **100**, 13.
8. Chumlyakov, Y. I., Surikova, N. S. and Korotaev, A. D., *Physics of Metals and Metallography*, 1996, **82**(1), 102.